JOURNAL OF MATERIALS SCIENCE **35** (2000) 5085–5090

An unusual behavior in the melting region of isotactic polypropylene crystals revealed by temperature-modulated DSC

A. TODA*, T. ARITA, M. HIKOSAKA
Faculty of Integrated Arts and Sciences, Hiroshima University, 1-7-1 Kagamiyama, Higashi-Hiroshima 739-8521, Japan
E-mail: atoda@hiroshima-u.ac.jp

We present a new method to analyze irreversible transformation kinetics of melting in polymer crystals with temperature modulated differential scanning calorimetry (TMDSC). In the melting region of several polymers, the apparent heat capacity obtained with TMDSC can be expressed as $C_s + (|F_{melt}|/\beta)/(1 + i\,\omega\,\tau(\beta))$, with the true heat capacity, C_s, the endothermic heat flow of melting, F_{melt}, the angular frequency of temperature modulation, ω, and the mean time of melting of each crystallite, τ, depending on the underlying linear heating rate, β. In the case of isotactic polypropylene, the frequency dependence cannot be approximated by this formula. The dependence suggests the possibility of the retardation in the melting kinetics to follow temperature modulation. © *2000 Kluwer Academic Publishers*

1. Introduction

Temperature-modulated DSC (TMDSC) [1–6] applies a periodic modulation in temperature to linear heating/cooling in a conventional DSC run and determines the complex heat capacity (apparent complex heat capacity in transition regions) from the heat flow response to temperature modulation. Fig. 1 shows typical results of TMDSC (total heat flow and the real and imaginary parts of apparent heat capacity) in the melting region of polymer crystals [7]. The total heat flow represents the heat flow averaged over one modulation period and corresponds to the heat flow obtained by a conventional DSC run. The complex heat capacity, $\widetilde{\Delta C}\,e^{-i\alpha}$, was determined from the amplitude and phase angle of modulation components in heat flow, $\dot{Q}$, and temperature, T_s, as follows,

$$T_s = \overline{T}_s + \mathrm{Re}\left[\widetilde{T}_s\, e^{i(\omega t+\epsilon)}\right], \tag{1}$$

$$\dot{Q} = \overline{\dot{Q}} + \mathrm{Re}[\widetilde{\dot{Q}}\, e^{i(\omega t+\delta)}], \tag{2}$$

$$C_0\, e^{-i\varphi} \equiv \frac{\widetilde{\dot{Q}}}{\omega\widetilde{T}_s}\, e^{-i(\epsilon-\delta-\frac{\pi}{2})} \Rightarrow \widetilde{\Delta C} e^{-i\alpha} \equiv \widetilde{\Delta C}' - i\,\widetilde{\Delta C}''. \tag{3}$$

Here, in the expression of the complex heat capacity, the arrow means that the calibration of the magnitude and phase angle is required for different modulation frequencies; the details of the calibration was discussed elsewhere [8].

In the melting region of polymer crystals, since polymer crystals are the aggregate of crystallites having a wide distribution of melting points, we can expect the quasi-steady response of total melting kinetics with the underlying linear heating even for quick melting of each crystallite. Therefore, the apparent heat capacity obtained in the melting region conveys important information about the melting kinetics. When examined at a certain fixed temperature, e.g. peak temperature, in the melting region of polymer crystals such as polyethylene [7], poly(ethylene terephthalate) [9] and nylon 6 [10], the frequency and heating rate dependences of the apparent heat capacity, such as shown in Fig. 1, could be roughly approximated by the frequency response function of Debye's type represented as,

$$\widetilde{\Delta C}\, e^{-i\alpha} = C_s + \frac{|F_{melt}|/\beta}{1 + i\omega\tau_0(\beta)}, \tag{4}$$

$$\tau_0 \propto \beta^{-x}, \quad 0.5 < x < 1, \tag{5}$$

with the true heat capacity, C_s, the endothermic heat flow of melting, F_{melt}, the angular frequency of temperature modulation, ω, and the characteristic time, τ_0, depending on the underlying linear heating rate, β.

We have proposed a modeling of the irreversible melting kinetics with linear heating for the aggregates of crystallites having a wide melting range [9, 7, 10, 11]. The modeling successfully explains the dependence represented in Equation 4 and gives the physical meaning for the characteristic time, τ_0, as the mean time of melting of each crystallite with underlying linear heating. It has been shown that the heating rate dependence of the mean time is determined by the

* Author to whom all correspondence should be addressed.

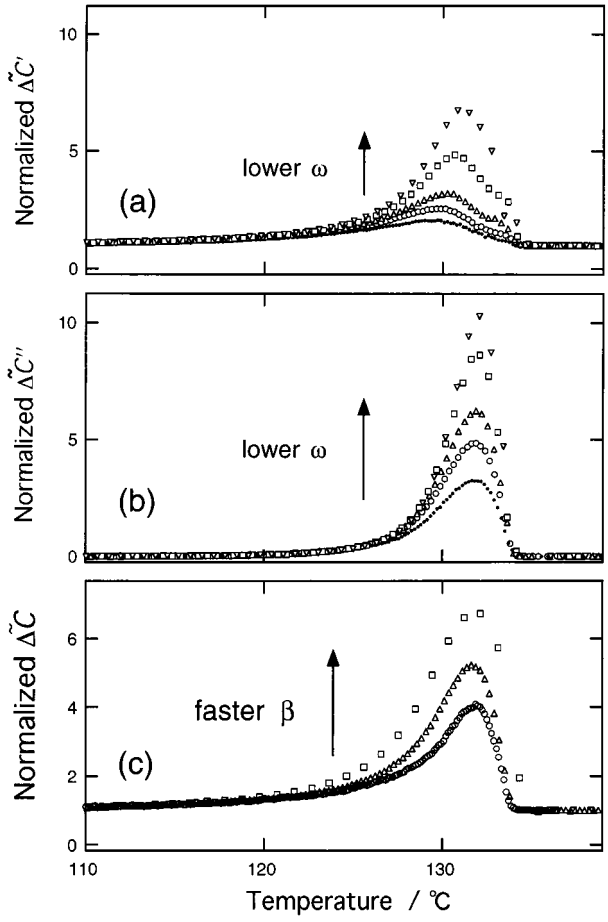

Figure 1 Apparent heat capacity in the melting region of polyethylene [7]. In (a) and (b), the underlying heating rate was 0.4 K min^{-1} and the modulation period was 28, 40, 52, 76 and 100 s. In (c), the underlying heating rate was 0.2, 0.4 and 1.5 K min^{-1} and the modulation period was 40 s.

superheating, ΔT, dependence of the melting rate coefficient, $R(\Delta T)$, of each crystallite, represented as,

$$R(\Delta T) \propto \Delta T^{y} \Rightarrow \tau_0 \propto \beta^{-y/(y+1)}. \qquad (6)$$

The superheating dependence of the melting rate coefficient becomes stronger than linear for $0.5 < x = y/(y+1)$ and indicates that the melting kinetics of polymer crystals requires an activation process such as nucleation for those polymers. By microscopy, it is difficult to examine the melting kinetics of each crystallite because polymer crystals are the aggregate of crystallites. Therefore, the information obtainable from TMDSC with the modeling is quite valuable in the investigation of melting kinetics.

In this paper, we examine the melting region of isotactic polypropylene (iPP) crystals, which has a relatively narrow melting range, *ca* 3 K, and hence the applicability of this technique applying a modulation must be carefully examined. Melting of iPP crystals is typical of polymer crystals showing double melting peaks, and the identification of the peaks has been a great issue in this field; the examination with TMDSC is expected to contribute to the better understanding of the processes.

In the following, we report an unusual behavior in the melting region which cannot be expected from the above modeling. The behavior can provide an opportunity to understand the melting behavior in more detail by incorporating other kinetic factors overlooked in the modeling.

2. Experimental

The DSC 2920 Module controlled with Thermal Analyst 2200 (TA Instruments) was used for all measurements. Helium gas with a flow rate of 4×10^{-5} m^3 min^{-1} was purged through the cell. The reference pan was removed to avoid introducing an uncontrollable parameter of the thermal contact between the reference pan and the base plate [12].

The polymer sample was a thin film of isotactic polypropylene (Montell SDK Sunrise Ltd., $M_w = 9.0 \times 10^4$ and the isotactic pentad fraction of $[mmmm] = 99.2\%$). The thickness and mass of the polymer film were 110 μm and 2.43 mg, respectively.

The sample was melted in an aluminum pan at 200°C and crystallized at temperatures in the range of 100–135°C. The melting behavior was examined with the underlying heating rate of 0.2, 0.4 and 0.8 K/min. Sinusoidal temperature modulation was applied with the modulation period in the range of 10–100 s and the amplitude satisfying heating only condition, $\frac{dT_s}{dt} > 0$, which is expressed as $\widetilde{T}_s < \frac{\beta}{\omega}$.

For the correction of complex heat capacity, the calibration coefficient of the magnitude has been adjusted for the data outside the transition region. Concerning the phase angle, a baseline has been chosen to set the phase angle to zero degrees outside the transition region. These approximations are justified for relatively small peaks of the apparent heat capacity, the condition of which is satisfied with smaller mass of sample [8]. A thinner sample of 22 μm and 0.48 mg was examined to see the effect of sample mass and thickness. It was confirmed that the behavior obtained with the thinner sample was essentially the same.

3. Results

Fig. 2 shows typical results of TMDSC in the melting region of iPP crystals. Like other polymers, the melting of iPP crystals showed strong dependence on frequency of the real and imaginary parts of the apparent heat capacity.

Narrow temperature width of the two melting peaks can be recognized in those figures. Due to the narrow temperature range, the response to temperature modulation can be out of steady state for longer than the modulation period even with a slow heating rate such as 0.8 K/min. The Lissajous diagram of the modulation components of heat flow and temperature actually shows the response out of steady state for longer modulation period, as shown in Fig. 3a. The condition out of steady state produces an artifact in the real part of the apparent heat capacity as a dip and peak corresponding to the steep rise and fall of the total heat flow shown in Fig. 2. This kind of artifact also appears in other polymers and has been confirmed by a numerical calculation based on the modeling of the melting kinetics with a finite distribution of melting points [11]. Therefore, this behavior is not special for iPP crystals.

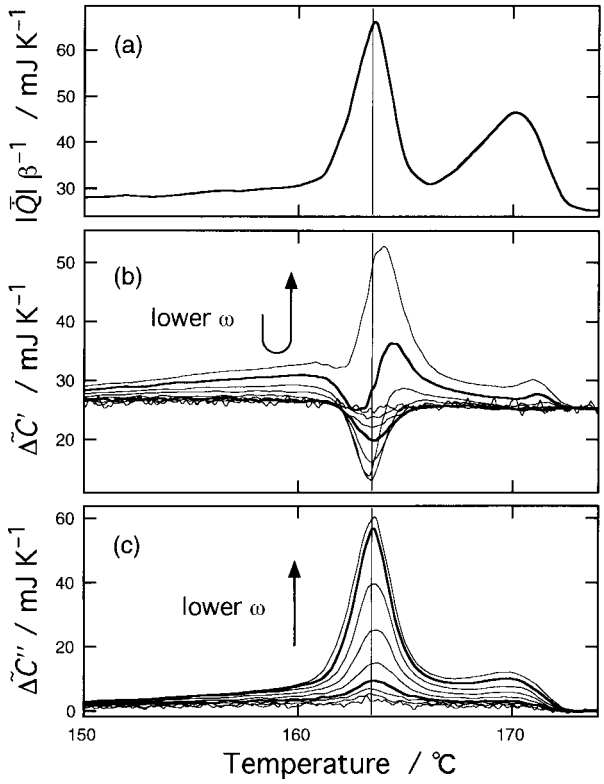

Figure 2 Total heat flow and apparent heat capacity in the melting region of iPP. The underlying heating rate was 0.8 K min^{-1} and the modulation period was 10, 17, 22, 28, 36, 47, 60, 78, 100 s. The two thick lines in (b) and (c) represent the results with the period of 28 and 78 s.

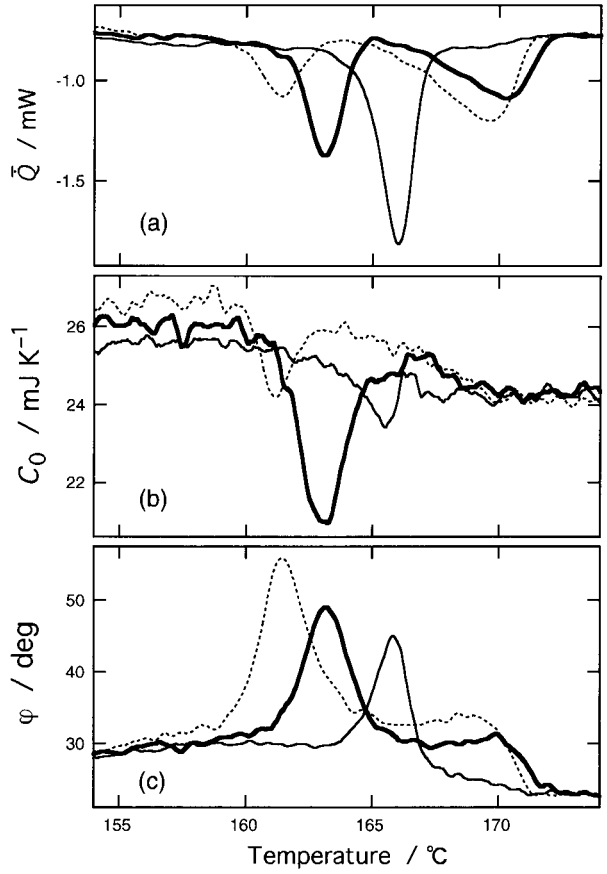

Figure 4 Total heat flow and the raw data of apparent heat capacity in the melting region of iPP crystallized at 115 (broken line), 125 (thick line) and 135°C (thin line). The underlying heating rate was 0.8 K min^{-1} and the modulation period was 28 s.

The unusual behavior with iPP crystals is the dip in the real part of the apparent heat capacity for shorter modulation periods, with which the Lissajous diagram shows a closed loop, as shown in Fig. 3b. It is further noted that the location of the dip corresponds to the peak in total heat flow, and hence it must be different from the dip obtained for longer modulation periods. A dip in the real part has been reported for polycaprolactone (PCL) crystals by Schawe *et al*. [13], but the condition of steady response was questioned. With the present evidences of the closed loop in the Lissajous diagram and the location of the dip corresponding to the peak in total heat flow confirm that the dip appears for the quasi-steady response in the melting region.

Besides the condition of steady response, we have to consider the influences of temperature gradient in the sample and the thermal contact between sample, sample pan and base plate of DSC. In order to examine those influences, the results with different crystallization temperatures for the same sample are shown in Fig. 4. It is clearly seen that the depth of the dips of the

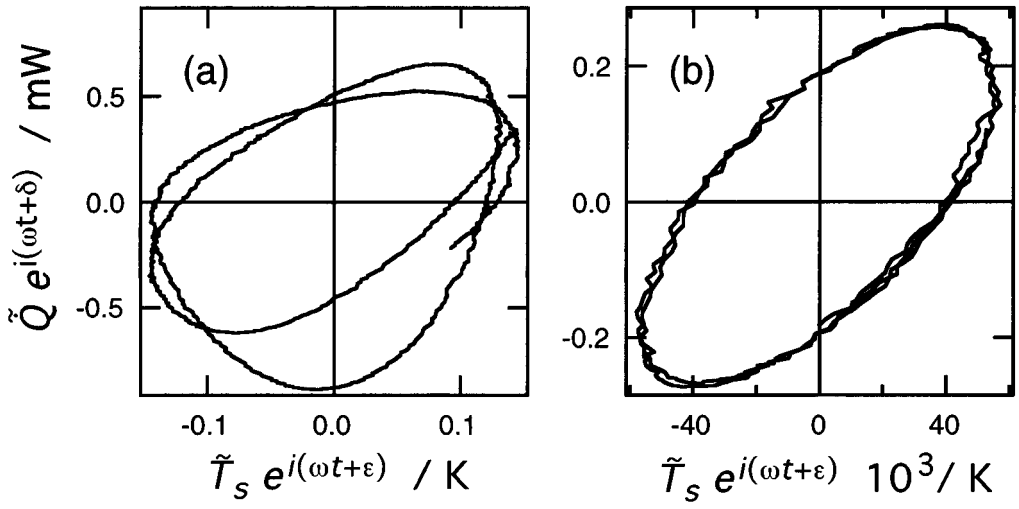

Figure 3 Lissajous diagrams of the modulation component of heat flow in the melting peak of Fig. 2 plotted against that of sample temperature. The two cycles are plotted. The modulation period in (a) and (b) is 78 and 28 s, respectively.

magnitude of apparent heat capacity changes with crystallization temperature and the direction of the change is independent of the change in the height of the peaks in total heat flow and in phase angle. Since the results were obtained with the same sample, the influences of the temperature gradient or the thermal contact will not be responsible for the systematic change in the depth of the dip which shows a maximum for the intermediate crystallization temperature. Therefore, the dip should be explained as the response of a kinetic contribution dependent on crystallization temperature.

4. Discussion

When compared at a fixed temperature, the frequency dependence of Fig. 2 is shown in Fig. 5. The dip in the real part is characterized as the systematic deviation from the hemi-circle in the Cole-Cole plot of Fig. 5c. The depth of dip becomes maximum at lower melting peak and becomes smaller at lower and higher temperatures; this behavior will be consistent with the maximum dip for the intermediate crystallization temperature shown in Fig. 4.

The following two expressions of the frequency response will be able to explain the dip in the real part, as shown in Fig. 6,

$$\widetilde{\Delta C} e^{-i\alpha} = C_s + \frac{A}{1+i\omega\tau_0} - \frac{B}{1+i\omega\tau_1}, \quad (7)$$

$$= C_s + \frac{A}{1+i\omega\tau_0}\frac{1}{1+i\omega\tau_1}, \quad (8)$$

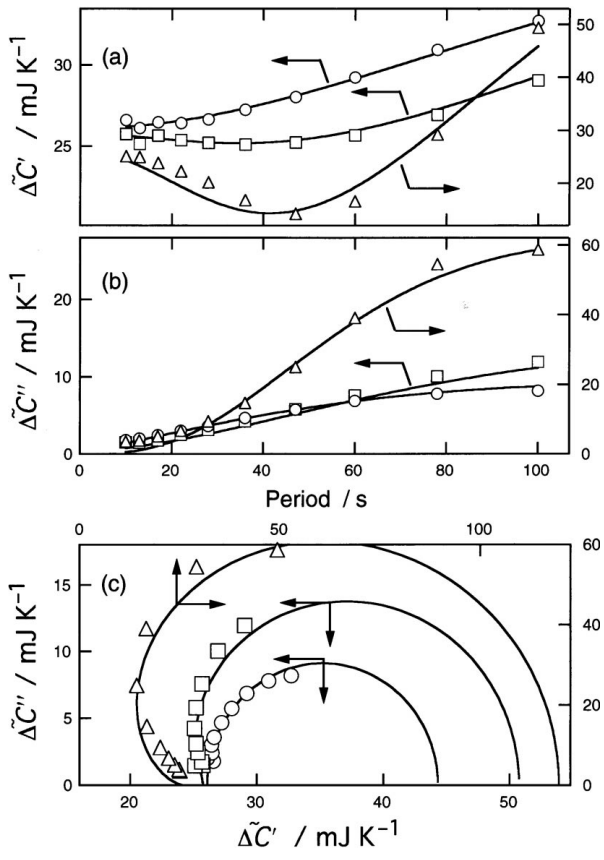

Figure 5 Frequency dependence of the complex heat capacity shown in Fig. 2 at respective temperatures of 160 (○), 163.5 (△) and 170°C (□).

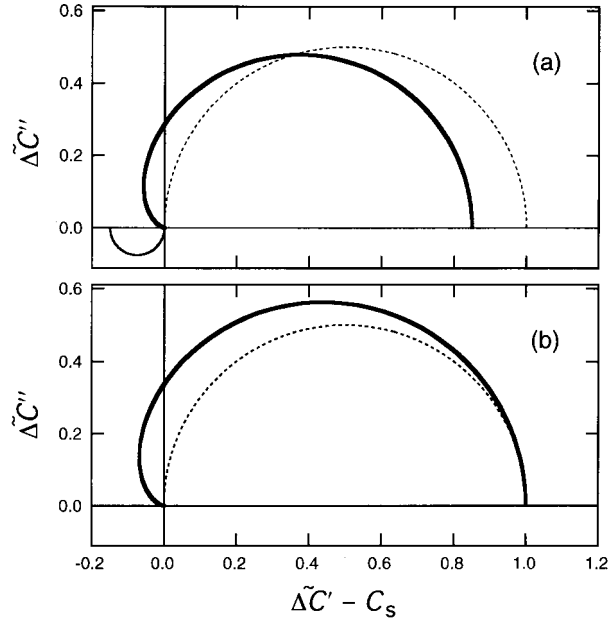

Figure 6 Schematic Cole-Cole plot of the apparent heat capacity obtained in the melting region of polymer crystals with different modulation frequency. The thick lines in (a) and (b) represent the plots of Equations 7 and 8, respectively, with $A = 1$, $B = 0.15$ and $\tau_1/\tau_0 = 0.15$. The thin line in (a) represents the plot of the third term in Equation 7. The frequency response function of Debye type was represented by broken line.

where A and B are constants and τ_1 represents a characteristic time introduced in the following modeling.

Firstly, Equation 7 represents the superposition of a new frequency response to the response of melting kinetics. In the melting region of polymer crystals, it is known that reorganization and/or recrystallization proceed as well as melting. In the melting region of polyethylene, poly(lethylene terephthalate) and nylon 6 crystals, the contribution has been neglected in our previous modeling because the response to temperature modulation is supposed to be negligibly small compared to that of melting, as is the case of crystallization. However, the superposition of frequency response of the kinetics to the response of melting can be a possible candidate for the unusual behavior. The contribution of kinetics to the apparent heat capacity is in general determined by the temperature dependence of kinetics represented as,

$$\widetilde{\Delta C}\, e^{-i\alpha} = C_s + \frac{i}{\omega} F_T', \quad (9)$$

where F_T' represents the temperature derivative of endo- or exo-thermic heat flow [14]. In order to produce the subtractive contribution of the third term in Equation 7, the sign of F_T' must be opposite to that of melting kinetics. When we take exotherm as positive heat flow, the sign of F_T' for the melting kinetics becomes negative with the rate increasing with temperature. For the exothermic process of recrystallization, the rate decreases with increasing temperature, and hence the sign is also negative. On the other hand, the exothermic process of reorganization is thermally activated with temperature increase. Therefore, F_T' of reorganization kinetics will take positive sign and can be responsible for the subtractive contribution. The process will

be enhanced at higher temperature, while the crystals formed at higher temperature will be less reorganized. Therefore, it is probable to have a maximum response of reorganization for the crystals formed in the intermediate temperature, as shown in Fig. 4. On the other hand, Fig. 2 suggests the location of the dip corresponding to the peak temperature in the endothermic heat flow. This result requires the correspondence of the reorganization peak with the melting peak, which needs further explanation. It should also be noted that, since the dip does not appear for $\tau_1/\tau_0 > 1$ as shown in Fig. 7, the condition for the dip with this model is expressed as $\tau_1/\tau_0 < 1$. However, it is not expected to find shorter mean time of completion for reorganization than for melting. The possibility of the frequency response of reorganization has those difficulties to explain the experimental results.

The second expression of Equation 8 represents the retardation of the melting rate in response to temperature change, as is schematically shown in Fig. 8. In this case, the contribution of kinetic response can be approximated as Equation 8 with the retardation time, τ_1; the details of the analysis will be discussed in a forthcoming paper [15]. Since the additional frequency response comes from the melting kinetics itself, the location of the dip must correspond with the peak temperature of heat flow. The heating rate dependence of the results in Cole-Cole plots shown in Fig. 9a also agree with the prediction of this model in Fig. 9b with constant retardation time, τ_1, and heating rate dependent mean time, τ_0. The fitting curve for the dip at 163.5°C in Fig. 5 represents the plot of Equation 8 with $C_s = 26$ mJ/K, $A = 94$ mJ/K and $\tau_0 \simeq \tau_1 \simeq 11$ s. From the frequency and heating rate dependences of the apparent heat capacity for $\omega\tau_0 \gg 1$, τ_0 for slower heating rate can also be determined by the plot shown in Fig. 10a with the

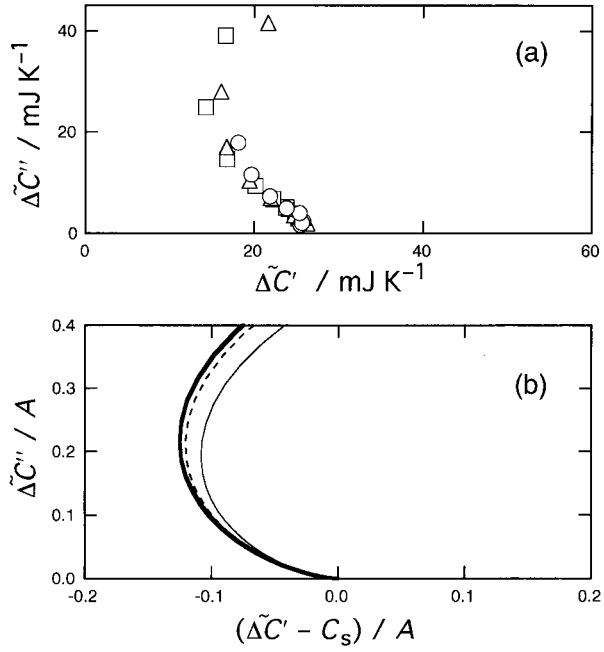

Figure 9 Cole-Cole plot of the apparent heat capacity in the melting region. The experimental results with heating rate of 0.2 (○), 0.4 (△) and 0.8 K/min (□) at respective peak temperatures of 164.2, 164.0 and 163.5°C are shown in (a). The calculated results of Equation. 8 for $\tau_1/\tau_0 = 0.41$ (thin line), 0.64 (broken line) and 1 (thick line) are shown in (b).

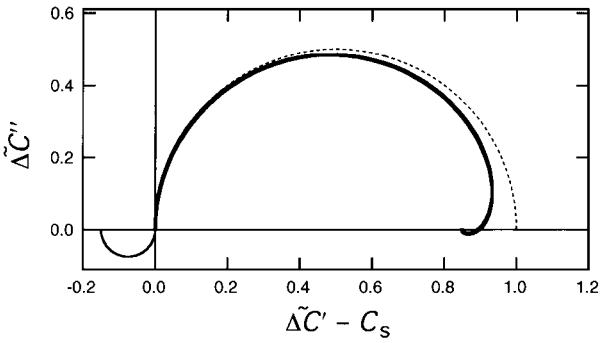

Figure 7 Schematic Cole-Cole plot of the apparent heat capacity representing the plots of Equation 7 for $A = 1$, $B = 0.15$ and $\tau_1/\tau_0 = 10$ (thick line). The meanings of thin and broken lines are the same as those in Fig. 6.

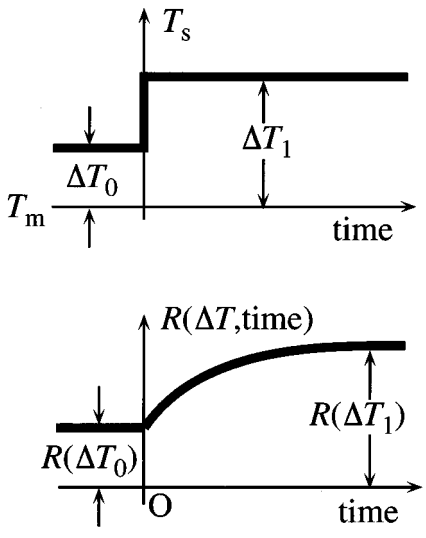

Figure 8 Schematic representation of the retardation behavior of melting rate coefficient responding to temperature change.

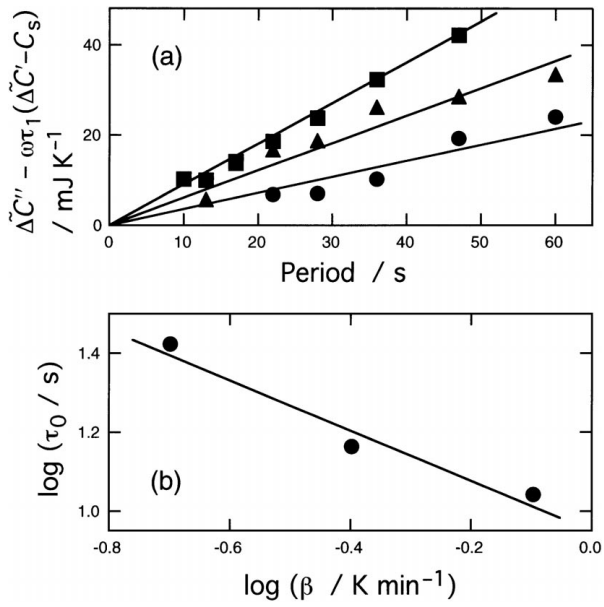

Figure 10 (a) Frequency dependence of the left hand side of Equation 10 with $\beta = 0.2$ (●), 0.4 (▲) and 0.8 K/min (■) at respective peak temperatures. (b) Heating rate dependence of τ_0 determined from the slope of the plots in (a), following the approximate form of Equation 10. The slope of the plot is −0.63.

following expansion of Equation 8 for $\omega\tau_0 \gg 1$,

$$\widetilde{\Delta C}'' - \omega\tau_1 (\widetilde{\Delta C}' - C_s) \cong \frac{A}{\omega\tau_0}. \qquad (10)$$

In Fig. 10a, τ_1 was assumed to be independent of heating rate and set at 11 s. From the slope of the plot and $\tau_0 = 11$ s at $\beta = 0.8$ K/min, τ_0 at 0.2 and 0.4 K/min has been determined as shown in Fig. 10b. The slope of the plot in Fig. 10b was -0.63 which was within the range reported for other polymers [7, 9, 10] shown in Equation 5. In Fig. 9b, this value of the exponent for τ_0 was assumed with $\beta = 0.2$, 0.4 and 0.8 K/min.

The retardation of melting rate coefficient indicates that the temperature dependent melting kinetics needs a reconstruction of the crystal-melt interface. The implication is in accordance with the activation process such as nucleation which is expected from the nonlinear dependence on superheating of melting rate coefficient expected from Equations 5 and 6. In terms of the maximum dip for the intermediate crystallization temperature, the reorganization of superheated crystallites will be possible and becomes most active for the intermediate crystallization temperature for the same reason mentioned in the first model. Under this situation, the retardation time required for the reconstruction of the interface will be longer and produce the maximum dip for the intermediate crystallization temperature because of the competition of melting with reorganization of superheated crystallites.

Concerning the double melting peaks shown in Fig. 2a, the response in the apparent heat capacity is much smaller for higher melting peak. The extrapolation of the Cole-Cole plot shown in Fig. 5c for $\omega \to 0$ gives $C_s + |F_{melt}|/\beta$ of pure melting from Equation 4. The extrapolated value for the higher melting peak actually corresponds to the value of the endothermic heat flow in Fig. 2a, and hence there will be no other processes in this temperature range. On the other hand, for the lower melting peak, the extrapolated value becomes much larger than the endothermic heat flow. In our previous work [7, 9, 10], we have shown that the difference is due to the exothermic heat flow of reorganization and/or recrystallization, both of which are insensitive to temperature modulation. Therefore, those behaviors clearly indicate that reorganization and/or recrystallization are most active in the temperature range of the lower melting peak, while those processes cease to occur at the higher melting peak; the possibility of this kind of differentiation is one of the advantages of TMDSC.

5. Conclusion

We have examined the dependence of the apparent heat capacity on the applied modulation frequency of TMDSC in the melting region of iPP crystals. The result showed the strong dependence of both the real and imaginary parts of complex heat capacity. We have confirmed the unusual behavior of the dip in the real part of the apparent heat capacity under quasi-steady state. The frequency dependence compared at fixed temperatures deviates from a hemi-circle in the Cole-Cole plot, while the dependence of polyethylene, PET and nylon 6 crystals were well approximated with the frequency dependence of Debye's type characterized by the hemicircle. The expressions of Equations 7 and 8 shown in Fig. 5 can explain the basic feature of the frequency response obtained with iPP crystals. Superposition of the frequency response of reorganization will result in the subtractive contribution of the third term in Equation 7 and the retardation of the response in melting rate to temperature change represents the frequency response of Equation 8. The explanation for Equation 7 requires the condition of $\tau_1/\tau_0 < 1$, but it is unlikely to predict a shorter mean time of completion for reorganization than for melting. Therefore, the most probable explanation will be based on the retardation of the response in melting rate to temperature modulation. The modeling with retardation can naturally explain the correspondence of the dip to the peak temperature of total heat flow. If the melting process competes with reorganization which will be most active in the intermediate temperature range, we also expect the maximum depth of the dip for intermediate crystallization temperature, which was observed experimentally. The retardation indicates the reconstruction of the interface and will also be related to the nonlinear dependence of melting rate on superheating. Therefore, the identification of the mechanism will be of great consequence in the understanding of the melting kinetics of polymer crystals.

Acknowledgements

The authors thank Mr. K. Yamada (Montell SDK Sunrise Ltd.) for his kind supply of isotactic polypropylene. This work was partly supported by a Grant-in-Aid for Scientific Research from the Ministry of Education, Science and Culture of Japan.

References

1. P. S. GILL, S. R. SAUERBRUNN and M. READING, *J. Therm. Anal.* **40** (1993) 931.
2. M. READING, D. ELLIOTT and V. L. HILL, *ibid.* **40** (1993) 949.
3. M. READING, A. LUGET and R. WILSON, *Thermochim. Acta* **238** (1994) 295.
4. B. WUNDERLICH, Y. JIN and A. BOLLER, *ibid.* **238** (1994) 277.
5. A. BOLLER, Y. JIN and B. WUNDERLICH, *J. Therm. Anal.* **42** (1994) 307.
6. I. HATTA, *Jpn. J. Appl. Phys.* **33** (1994) L686.
7. A. TODA, C. TOMITA, M. HIKOSAKA and Y. SARUYAMA, *Thermochim. Acta* **324** (1998) 95.
8. A. TODA, T. ARITA, C. TOMITA and M. HIKOSAKA, *Polymer*, in press.
9. A. TODA, C. TOMITA, M. HIKOSAKA and Y. SARUYAMA, *Polymer* **39** (1998) 5093.
10. *Idem., J. Therm. Anal.* **51** (1998) 623.
11. A. TODA, T. ARITA, C. TOMITA and M. HIKOSAKA, *Thermochim. Acta* **330** (1999) 75.
12. I. HATTA and S. MURAMATSU, *Jpn. J. Appl. Phys.* **35** (1996) L858.
13. J. E. K. SCHAWE and E. BERGMANN, *Thermochim. Acta* **304/305** (1997) 179.
14. A. TODA, T. ODA, M. HIKOSAKA and Y. SARUYAMA, *ibid.* **293** (1997) 47.
15. A. TODA and Y. SARUYAMA, *Polymer*, submitted.

Received 31 January
and accepted 25 February 2000